13.7 A 10Gb/s Photonic Modulator and WDM MUX/DEMUX Integrated with Electronics in 0.13μm SOI CMOS

Andrew Huang, Cary Gunn, Guo-Liang Li, Yi Liang, Sina Mirsaidi, Adithyaram Narasimha, Thierry Pinguet

Luxtera, Carlsbad, CA

Integration of optical functions with CMOS electronics provides a low-cost solution for high-bandwidth fiber-optic links. Prior silicon modulators have been limited to <1GHz bandwidth [1]. Recent efforts have achieved 10Gb/s, but lacked process integration with electronics [2, 3]. In this paper, manufacturable yield-friendly photonics components combined with electronics using a 0.13μm SOI process for PowerPC™ processors are described. A 10Gb/s optical modulator integrated with a driver and a 4-channel WDM MUX/DEMUX with integrated tuning circuits that improve manufacturing yield and crosstalk, is presented.

C-band (1.5μm) optical waveguides are formed by a high refractive index core of transparent silicon and a cladding of lower refractive index silicon dioxide. The bottom cladding is the buried oxide layer found in the SOI wafer; the top cladding is the first ILD, and the lateral cladding is the field oxide used to isolate transistors.

A holographic lens (HL) couples light normal to the surface of the die with <1.5dB loss. HL coupling also allows inexpensive wafer scale testability, a significant cost advantage. Figure 13.7.1 shows an SEM of a fabricated HL and demonstrates how a fiber can be used to illuminate the HL.

The modulator uses a free-carrier-effect-based device in a Mach-Zehnder interferometer (MZI). The MZI is intuitively simple: light is split evenly into two arms, and then recombined. Along each of the two arms, the light is phase-modulated (delayed). Differential accumulation of phase ($\Delta\phi$) along each arm causes the recombined light to interfere according to the interferometer equation, $P = 0.5 + \cos(\pi/2 + \Delta\phi)/2$.

The effect used to modulate optical phase is based on free-carrier plasma dispersion [4]. The transducer is a reverse-biased lateral PIN diode. High-speed modulation is obtained as majority carriers are swept in and out of the optical mode by electrical fields. Thus, the speed of the resulting device is entirely limited by RLC parasitics. This is in contrast to conventional methods based on diffusion/recombination processes of minority carriers in a forward-biased diode. Figure 13.7.2 depicts the phase modulator in one MZI arm.

In a lumped configuration, the junction length needed for sufficient phase shift would be parasitic-limited to <10Gb/s. One way to overcome this lumped-RC speed limit is to design a traveling-wave electrode. The modulation waveguide with its PN junction is designed as part of the microwave transmission line. The geometry of the microwave transmission line is chosen such that the electrical group delay and the optical phase velocity are approximately matched. On-chip terminations are integrated at the end of the microwave transmission lines to suppress back-reflections.

The characteristic impedance of the transmission line itself is >25Ω, but when loaded with the PIN diode, the total system achieved 25Ω. The modulator has a length of 2mm, also chosen to ensure that microwave loss would be sufficiently small to obtain a large bandwidth, and that optical insertion loss would be small. At the same time, the 2mm modulator achieves enough phase shift for a favorable extinction ratio at a performance of ~5°/mm/V/arm.

A cascoded *thin*-gate-oxide transistor switch is used at the core of the integrated high-speed modulator driver. A schematic of the driver circuit is shown in Fig. 13.7.3. A pre-driver chain drives the switch transistor, and the cascode device is used to shield the high-performance switch from the relatively high voltages required by the modulator elements. The pull-down switch is used in conjunction with the far-side termination resistor of the CPW transmission line of the MZI device to complete the driver circuitry.

The integrated MZI modulator plus driver yields a 10^{-12} BER with a 2^{23}-1 PRBS at 10Gb/s. Figure 13.7.4 presents the received optical eye diagram at 10Gb/s. The MZI is biased at quadrature. Performance of the optical modulator is entirely limited by the characteristics of this driver. The device is tested on-wafer using an electro-optical probe card arrangement. The active area for the modulator driver is 0.08mm^2 and the total area is 2.6mm^2 including the 2mm modulator, the termination network, and the pads.

A key advantage of integrated electronics and photonics on a single chip is to raise yield of an optical device by electronic control circuitry that compensates process-induced errors. To this effect, an optical 4-channel DWDM AWG with an 8b DAC array is integrated in the same process. The die mircograph is shown in Fig. 13.7.5. The entire AWG plus DAC array is <0.6mm^2 in area.

The ability of AWG to generate a desired spectral function depends on the phase relationship between arrayed waveguides. Errors in fabrication of optical waveguides cause changes in their structure that induce random delays to the optical signal. This results in a degraded phase relationship between the waveguides, manifesting itself as crosstalk.

Forward-biased PIN junction phase modulators integrated into each arm of the AWG are used to restore the phase relationship. Forward-biased PIN modulators offer greater phase efficiency (90°/mA for a 100μm arm) at the cost of lower speed and higher loss when compared to reverse-biased PIN modulators. Each modulator is driven by an 8b 5/3 segmented DAC. The entire current source array is constructed using I/O-type transistors with body ties. The layout is optimized to enable the DAC to be pitch-matched to the AWG phase modulator array for easy integration.

Figure 13.7.6 shows the spectral response of the AWG before and after tuning. The filter function is recovered and the crosstalk suppression is improved by over 16dB. This demonstrates that the on-chip DAC is able to recover a usable filter function from a previously defective AWG. In addition to yield enhancement, this same calibration mechanism is used to compensate for environmentally induced thermal offset during device operation.

Acknowledgements:
The authors would like to thank Behnam Analui, Erwin Balmater, Drew Guckenberger, Mark Harrison, Ryan Ingram, Daniel Kucharski, and the whole Luxtera team for making this paper opportunity possible. We would also like to thank Jagdeep Shah and DARPA for support under the EPIC program.

References:
[1]. A. Irace, et al., "A. Fast Silicon-on-Silicon Optoelectronic Router Based on a BMFET Device," *IEEE J. Select. Topics Quant. Elec.*, vol. 6, pp. 14-18, 2000.
[2]. C.A. Barrios, et al., "Electrooptic Modulation of Silicon-on-Insulator Submicrometer-Size Waveguide Devices," *IEEE J. Lightwave Technol.,* vol. 21, pp. 2332-2339, 2003.
[3]. L. Liao, et al., "High speed silicon Mach-Zehnder modulator," *Optics Express,* vol. 13, pp. 3129-3135, 2005.
[4]. R.A. Soref and B.R. Bennett, "Electrooptical Effects in Silicon," *IEEE J. Quant. Elec.,* vol. 23, pp. 123-129, 1987.

 1-4244-0079-1/06 ©2006 IEEE

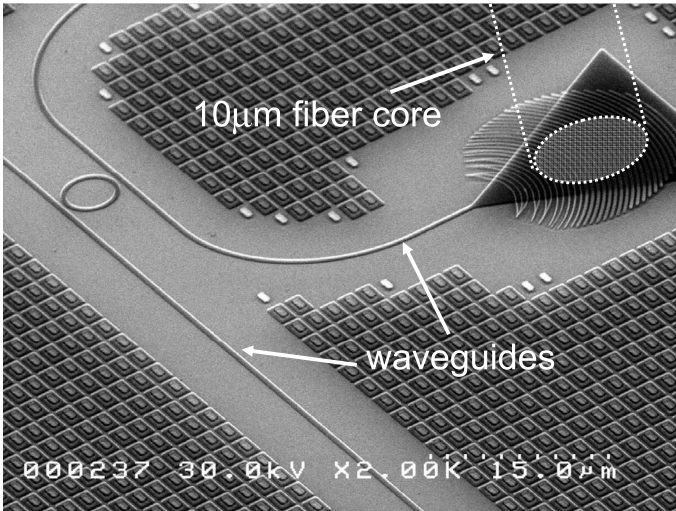

Figure 13.7.1: SEM photograph of a holographic lens (upper right corner). Light is coupled from the optical fiber into the waveguides or vice-versa.

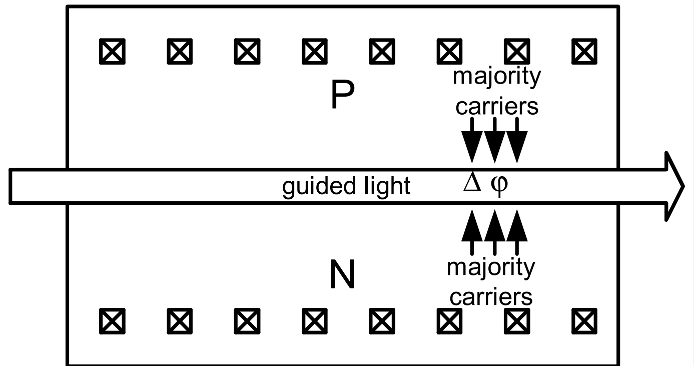

Figure 13.7.2: Schematic diagram of a phase modulator in one arm of the MZI.

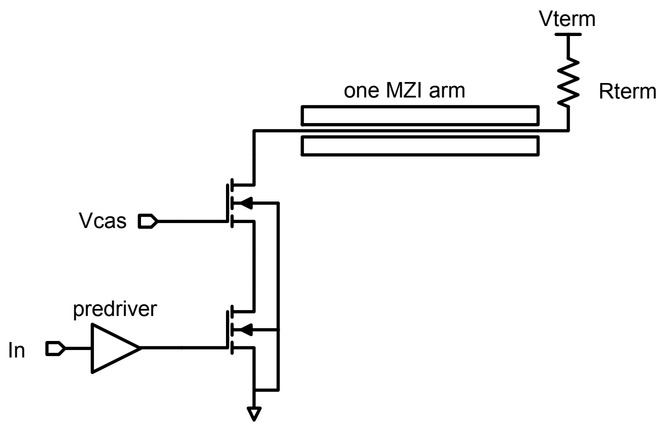

Figure 13.7.3: Integrated driver connected to one MZI arm.

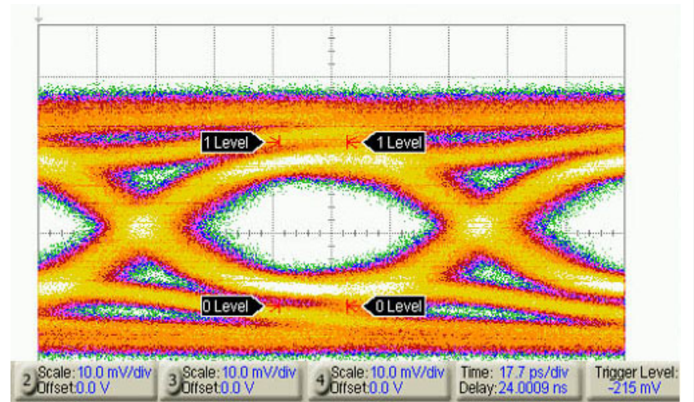

Figure 13.7.4: Optical eye of integrated modulator plus driver at 10Gb/s.

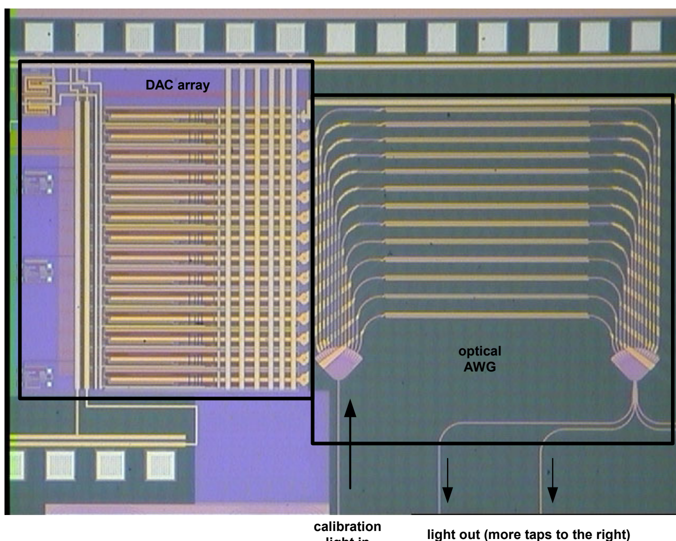

Figure 13.7.5: Die shot of DAC array plus AWG element.

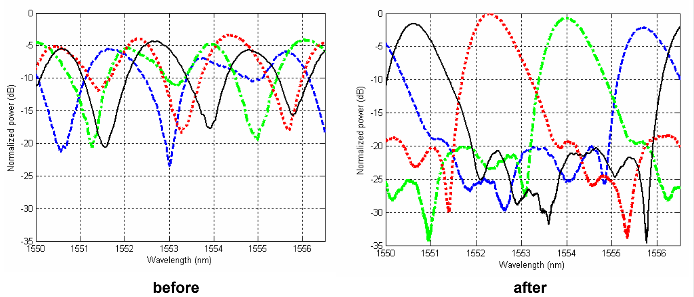

Figure 13.7.6: AWG transfer functions before and after tuning with an array of integrated DACs.

1-4244-0079-1/06 ©2006 IEEE

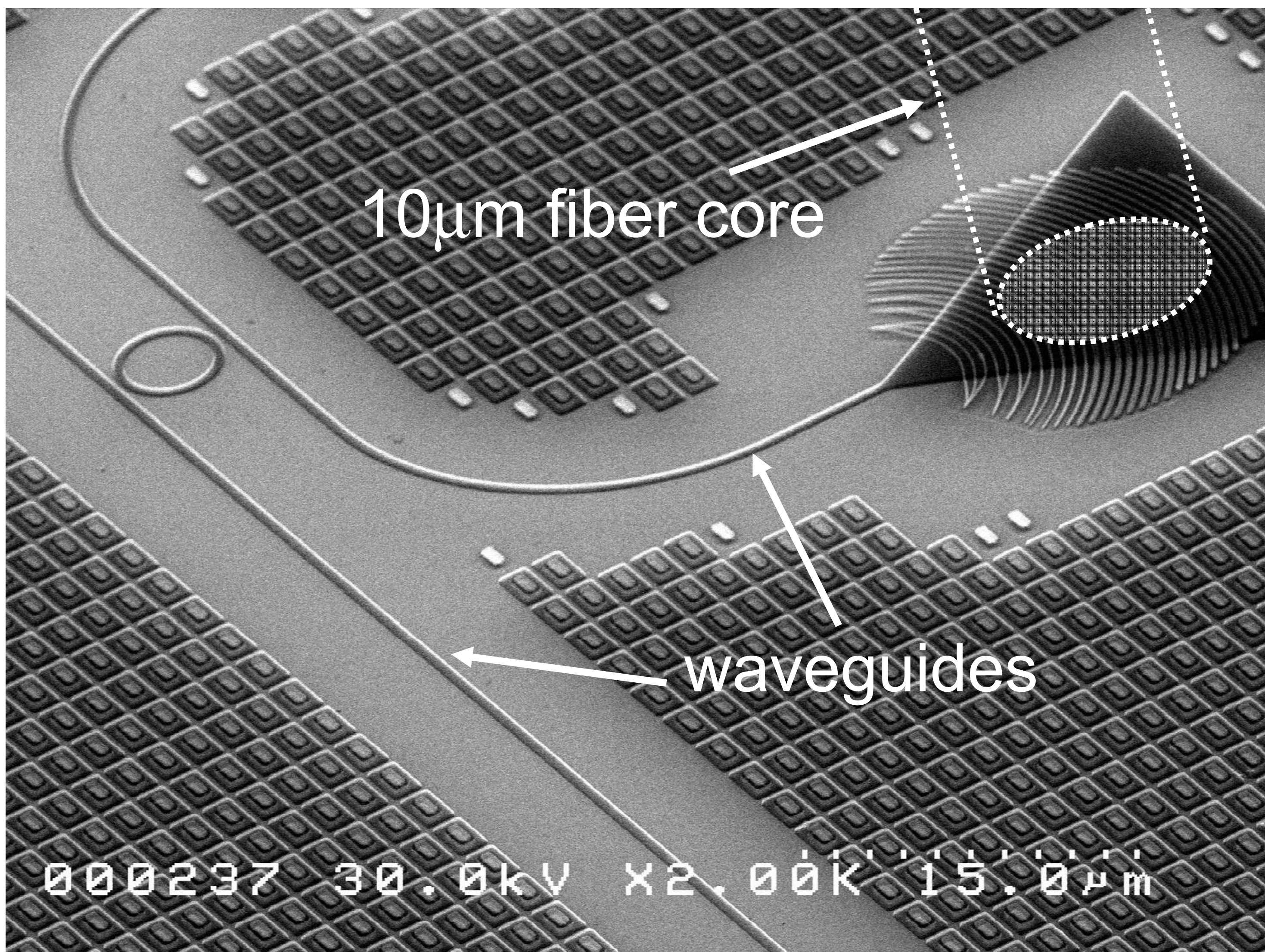

Figure 13.7.1: SEM photograph of a holographic lens (upper right corner). Light is coupled from the optical fiber into the waveguides or vice-versa.

 1-4244-0079-1/06 ©2006 IEEE

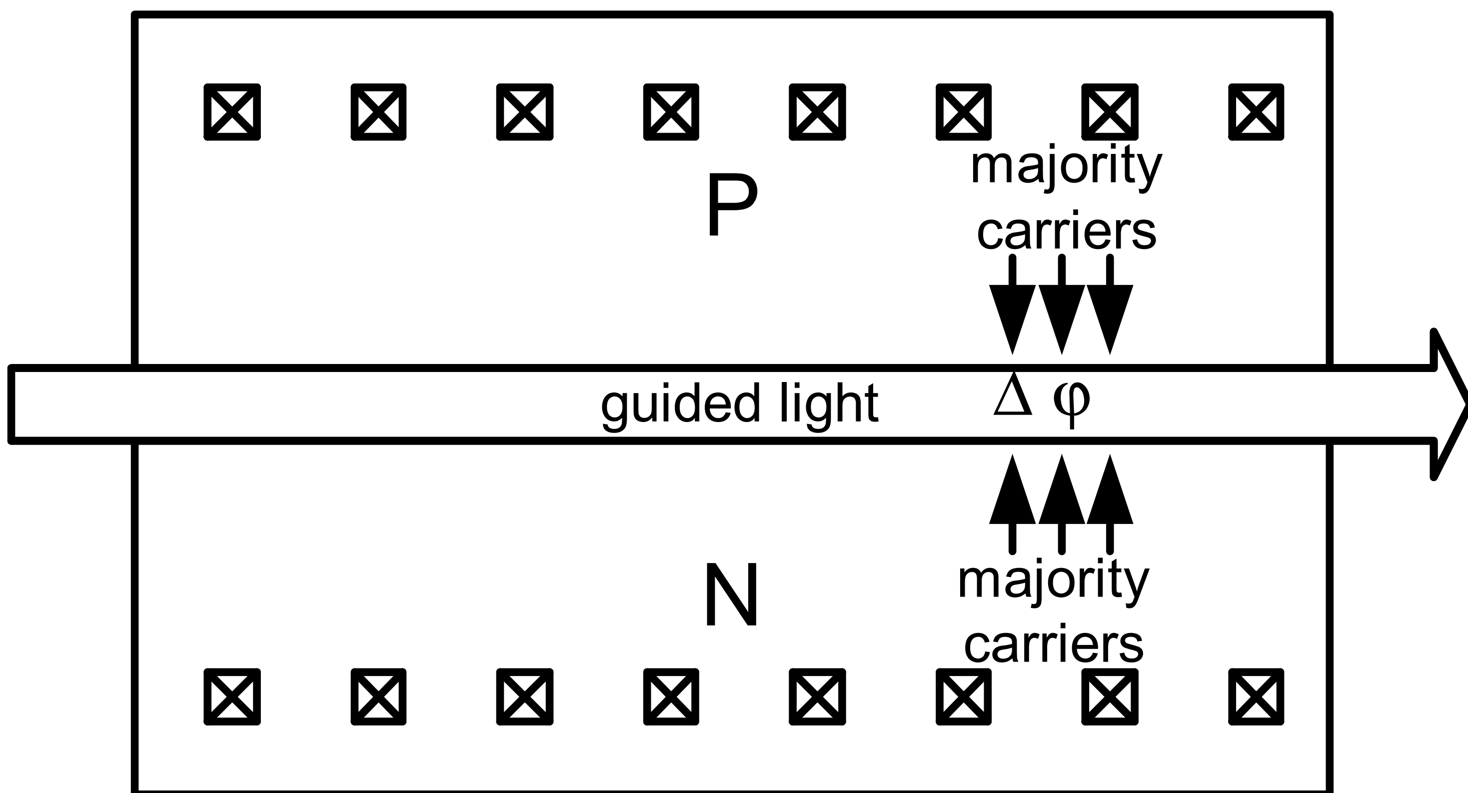

Figure 13.7.2: Schematic diagram of a phase modulator in one arm of the MZI.

1-4244-0079-1/06 ©2006 IEEE

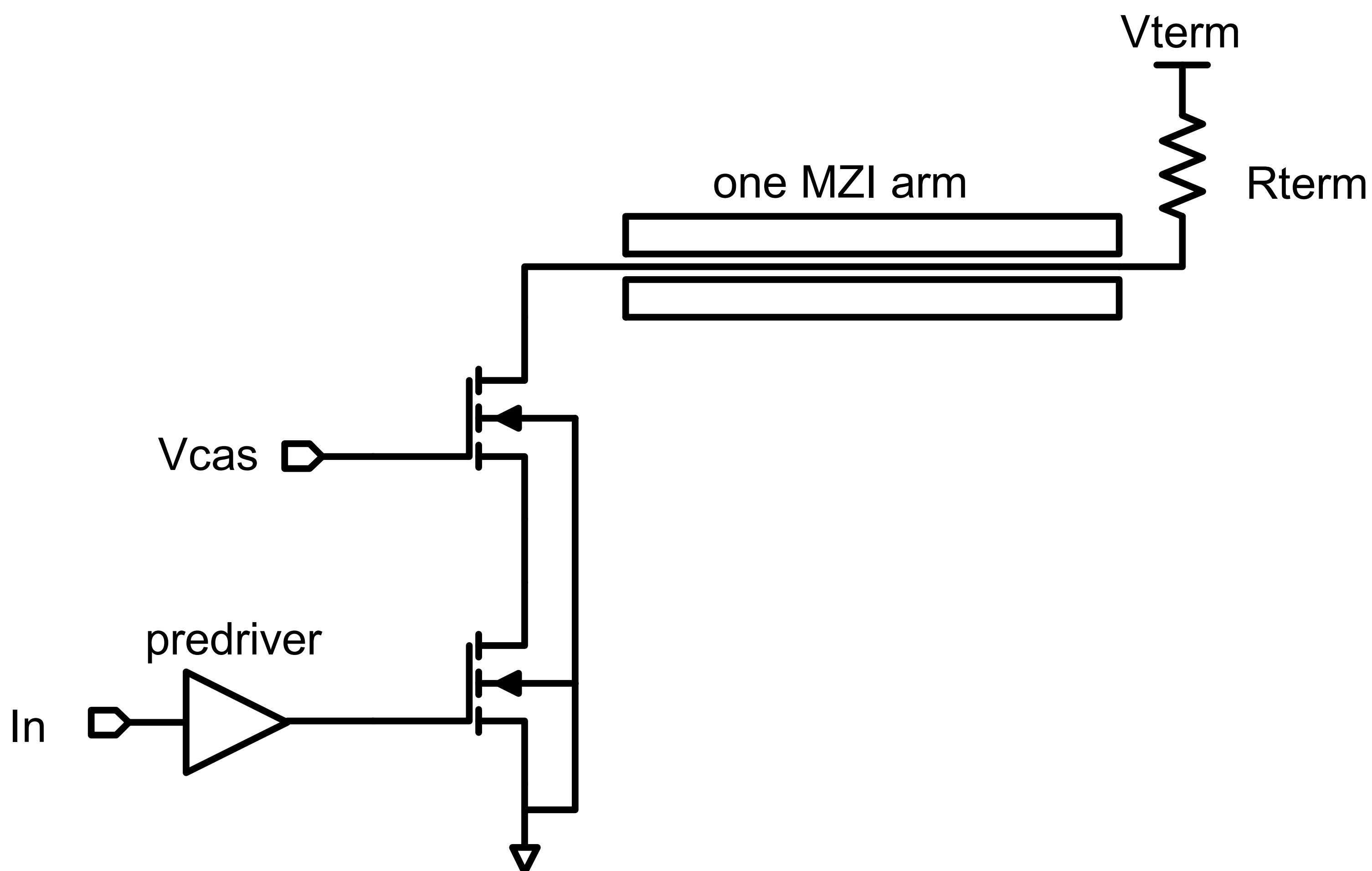

Figure 13.7.3: Integrated driver connected to one MZI arm.

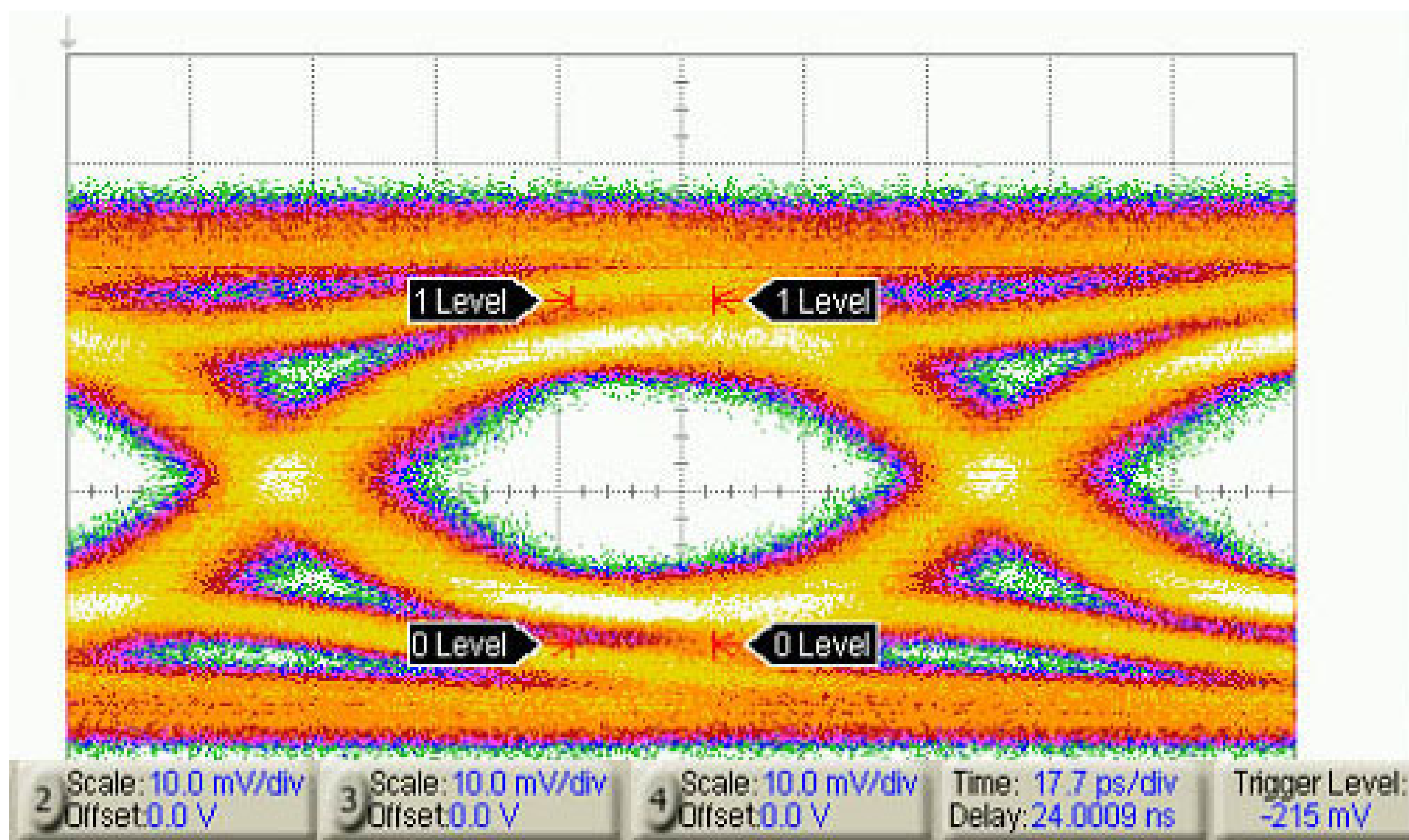

Figure 13.7.4: Optical eye of integrated modulator plus driver at 10Gb/s.

1-4244-0079-1/06 ©2006 IEEE

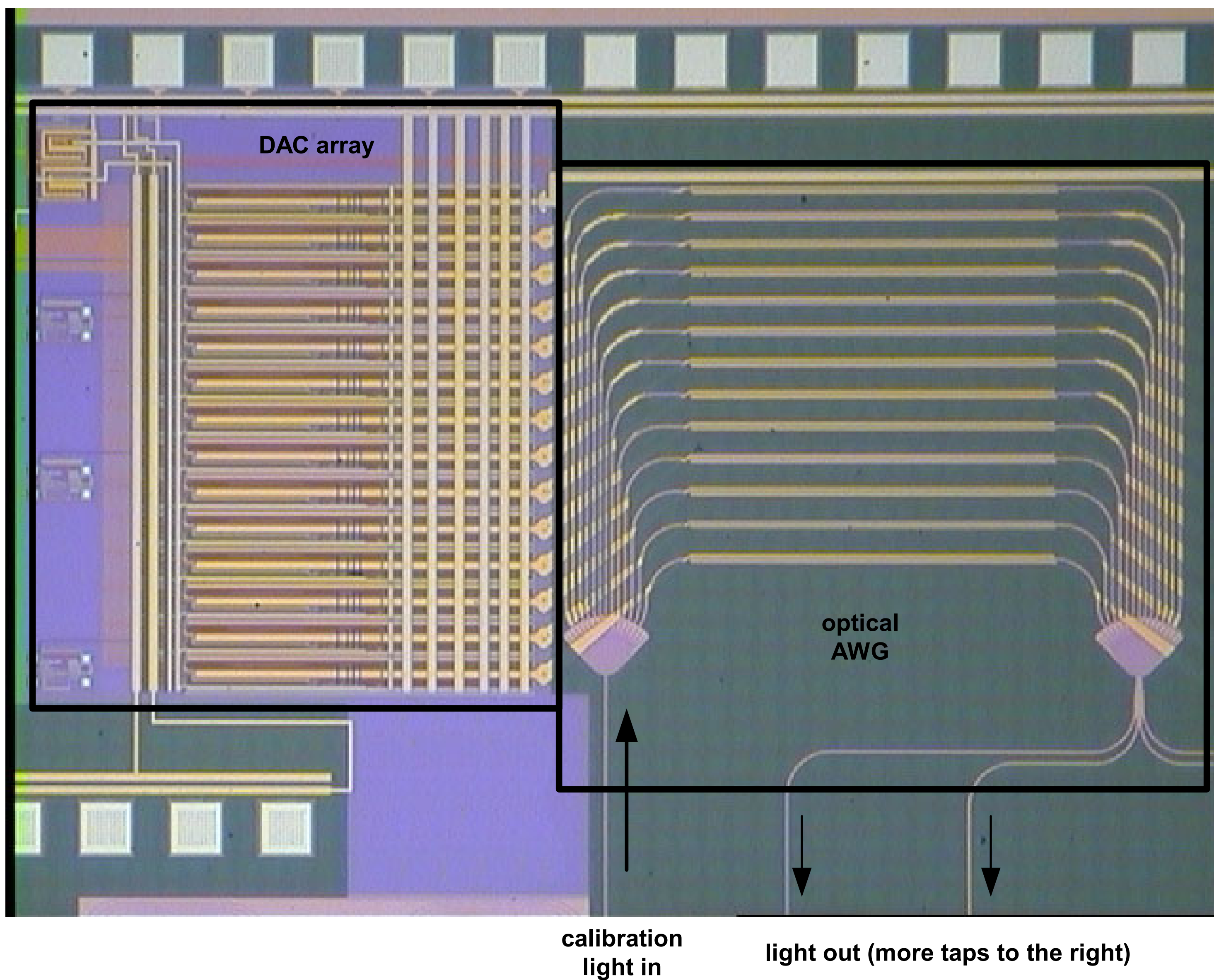

Figure 13.7.5: Die shot of DAC array plus AWG element.

1-4244-0079-1/06 ©2006 IEEE

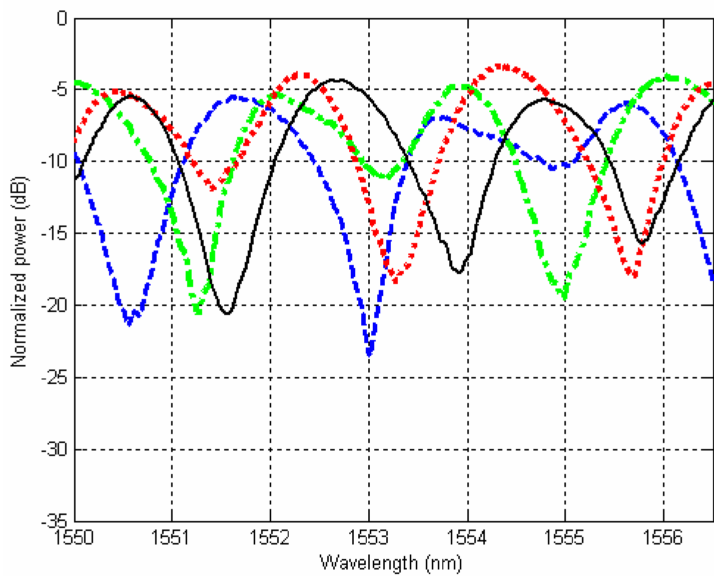

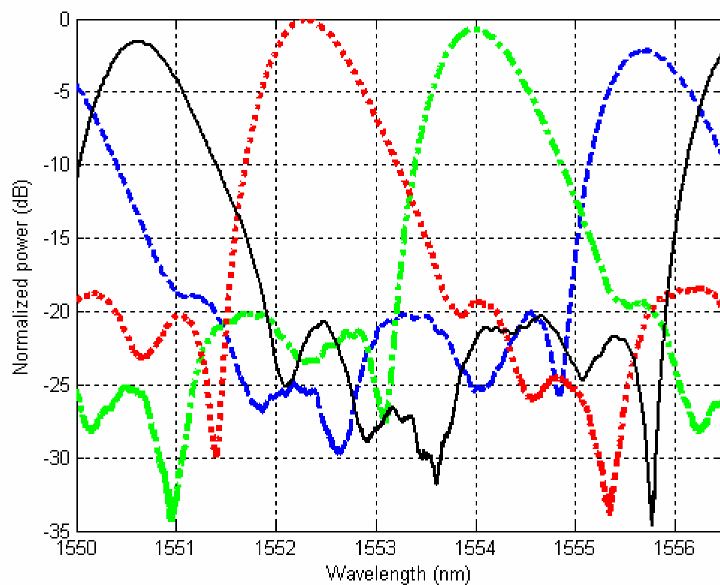

before **after**

Figure 13.7.6: AWG transfer functions before and after tuning with an array of integrated DACs.

1-4244-0079-1/06 ©2006 IEEE